# A Comparative Study of 3D Printed Bowtie and Monopole Antennas for Ka-Band


Md Mufassal Ahmad
Department of Electrical Engineering
University of North Texas
Denton, TX 76207, USA
mdmufassalahmad@my.unt.edu

Jun Ying Tan
Department of Electrical Engineering
University of North Texas
Denton, TX 76207, USA
junyingtan@my.unt.edu

Son Vu
Department of Electrical Engineering
University of North Texas
Denton, TX 76207, USA
SonVu@unt.edu

Cheolbok Kim
Corning Incorporated
Corning
Painted Post, NY 14870, USA
kimc4@corning.com

Hung Luyen
Department of Electrical Engineering
University of North Texas
Denton, TX 76207, USA
Hung.Luyen@unt.edu

Jungkwun 'JK' Kim
Department of Electrical Engineering
University of North Texas
Denton, TX 76207, USA
Jungkwun.Kim@unt.edu



2024 IEEE 17th Dallas Circuits and Systems Conference (DCAS) | 979-8-3503-4953-5/24/$31.00 ©2024 IEEE | DOI: 10.1109/DCAS61159.2024.10539860



**Abstract— This study demonstrates the feasibility of fabricating Ka-band antennas using digital light processing (DLP) 3D printing technology, with a focus on integrating DLP 3D printing with conventional micromachining processes. We successfully designed and printed air-lifted 3D bowtie and monopole antennas on a photosensitive resin substrate. The antennas were designed to resonate at 28 GHz for advanced 5G wireless communications. The monopole antenna, with a height of 2.67 mm and a diameter of 500 µm, achieved a resonant frequency of 27.9 GHz, an input reflection coefficient of -26.6 dB, and a maximum realized gain of 6.19 dBi. The bowtie antenna, featuring a height of 1.67 mm, a top width of 2 mm, a bottom width of 300 µm, and a flare angle of 30°, also resonated at 27.9 GHz with an input reflection coefficient of -51.1 dB and a gain of 5.48 dBi. These results highlight the potential of DLP-based 3D printing to create effective and customizable antenna solutions for the rapidly evolving demands of modern wireless networks.**



***Keywords— Air-lifted antenna, Bowtie antenna, Monopole antenna, Ka-band, 3D printing.***


## I. INTRODUCTION

Antennas operating within the Ka-band frequency range (26.5-40 GHz) are pivotal for the advancement of 5G wireless communication networks. This frequency spectrum offers significantly wider bandwidths than traditional cellular bands, facilitating the high data rates and low latency required by emerging 5G applications [1, 2]. Common 2D PCB-based antennas in 5G networks, such as patch, slot, and dipole antennas, are relatively simple to fabricate [3-5]. Although simple to fabricate, these antennas' large contact area with the substrate leads to higher dielectric losses, reducing their efficiency.

3D printing offers unprecedented design freedom in antenna fabrication, enabling complex geometries unachievable through conventional methods. Examples of 3D-printed antennas include helical antennas, fractal antennas, and dielectric resonator antennas [6-9]. However, 3D-printed antennas within the Ka-band for 5G are still relatively unexplored.

Integrating conventional micromachining processes with 3D printing allows for fabricating intricate 3D antenna structures. This hybrid approach leverages the strengths of both techniques, such as enhanced resolution from 3D printing and precision from micromachining, enabling the fabrication of antennas with significantly improved efficiency and bandwidth.

This study investigates the feasibility of fabricating complex Ka-band antenna designs using a hybrid 3D printing and microfabrication approach. Inspired by a recent study demonstrating the advantages of an air-lifted monopole-type bowtie antenna [10], we adopted this design and targeted a resonant frequency of 28 GHz. Our fabrication process builds upon this earlier work [11, 12], but streamlines it significantly. We integrate 3D printing, DC sputtering, lift-off, and electroplating, eliminating the need for high-skilled labor-intensive processes like precise shadow mask alignment, lithography, and laser machining. This approach seamlessly merges conventional microfabrication with 3D printing advantages and explores the use of unconventional dielectric materials (3D printable photosensitive resin) as antenna substrates. Our method reduces the antenna's surface-to-volume ratio, which enhances operational efficiency and supports the development of high-frequency Ka-band antennas for advanced 5G applications.

## II. ANTENNA DESIGN AND SIMULATION

The Ka-band, covering frequencies from 26.5 GHz to 40 GHz and corresponding to wavelengths between 1.1 cm and 0.75 cm, presents unique challenges for antenna fabrication. Traditional manufacturing methods, such as milling or machining, struggle with these dimensions, as they are too small for efficient processing but too large for conventional micromachining techniques. As such, the precision required to meet half or quarter wavelength specifications for optimal antenna performance cannot be easily achieved. In this context,


979-8-3503-4953-5/24/$31.00 ©2024 IEEE

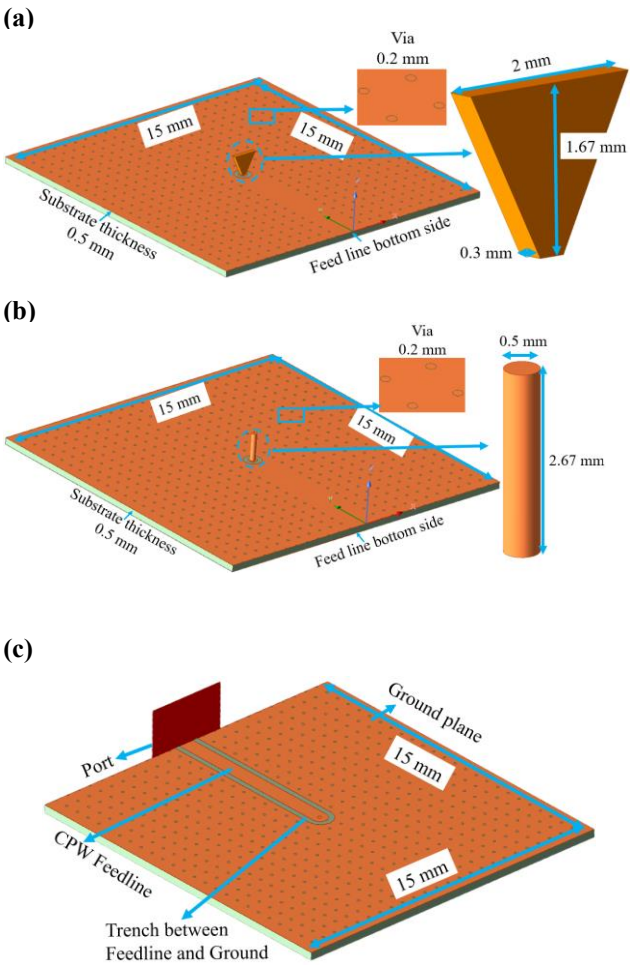


Fig. 1. Structures of the 3D-printed (a) bowtie antenna (b) monopole antenna, and (c) backside of substrate for both antennas.

advanced 3D printing technologies, particularly DLP printers, become very useful. These printers offer the necessary resolution, typically ranging from a few tens to a few hundred microns, enabling the accurate fabrication of antennas suited for the compact wavelength dimensions of the Ka-band. This section details the design considerations and simulation processes undertaken to develop antennas capable of exploiting the full potential of the Ka-band's high-frequency spectrum.

Traditional bowtie antennas are typically constructed with two triangular plates positioned on a printed wire board (PWB) substrate [13]. These plates are symmetrically arranged and connected via a two-wire transmission line, which occupies considerable space. In a recent advancement, an innovative design of an air-lifted bowtie antenna was introduced [10]. This design, a monopole variant of the traditional bowtie, was fabricated using 3D microlithography and micromachining processes, achieving a resonant frequency of 12.34 GHz. This antenna features a single triangular plate oriented vertically above a ground plane, with one vertex connected to a coplanar waveguide.

In our study, we adopted a similar air-lifted bowtie antenna design, fabricated on a substrate composed of an unconventional dielectric material—3D printing resin. Utilizing advanced 3D

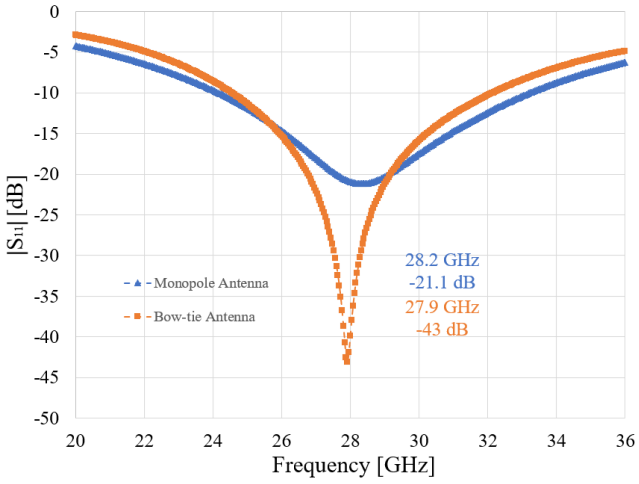


Fig. 2. HFSS simulated input reflection co-efficient $|S_{11}|$ [dB] results of the 3D monopole and bow-tie antenna.

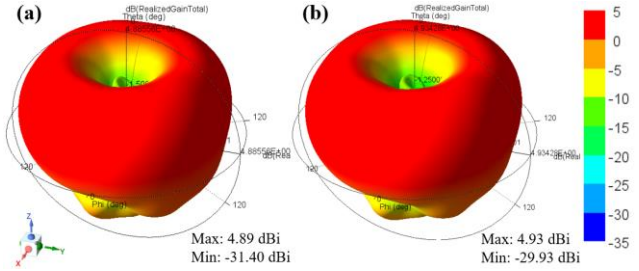


Fig. 3. Simulated 3D radiation patterns of the (a) bowtie antenna and (b) monopole antenna.

printing and metallization techniques, we fabricated the antenna on a substrate made from a photosensitive resin (Green Translucent UV Resin, Anycubic), known for its effective dielectric constant ranging between 2.9 and 3.1 [14]. We designed a bowtie antenna with a height of 1.67 mm, a thickness of 0.3 mm, and a top width of 2 mm to match the quarter wavelength for 28 GHz, incorporating a flare angle of 30° as depicted in Fig. 1(a). Concurrently, a monopole antenna was developed for a resonant frequency of 28 GHz, featuring a height of 2.67 mm and a diameter of 0.5 mm, illustrated in Fig. 1(b).

Both antennas were positioned on a square-shaped substrate measuring 15 mm × 15 mm, with a thickness of 0.5 mm as shown in Fig. 1(c). A coplanar waveguide (CPW) was strategically placed at the center of the substrate, measuring 7.5 mm in length and 1.2 mm in width. The gap between the ground plane and the CPW line is 0.5 mm wide with a trench depth of 0.2 mm. Additionally, the antenna assembly on the substrate's backside includes a 100 µm deep island, effectively isolating the antenna from the ground. To achieve optimal impedance matching and meet the skin depth requirement, a 2 µm-thick copper layer was essential for constructing a 50-ohm CPW line.

The abovementioned designs were simulated using Ansys high-frequency structure simulator (HFSS), and the simulation results are shown in Fig. 2. The simulation results showed an input reflection coefficient $|S_{11}|$ of -43 dB at 27.9 GHz for the bowtie antenna and $|S_{11}|$ of -21.1 dB at 28.2 GHz for the

monopole antenna. The simulated 3D radiation pattern of the two antennas, presented in Fig. 3(a, b), are like each other. The peak realized gains of the bowtie and monopole antennas are 4.89 dBi and 4.93 dBi, respectively.

## III. Fabrication Process

Fig. 4 depicts the key fabrication processes of the 3D-printed bowtie antenna. The process began by 3D printing the bowtie antenna using a digital light processing (DLP)-based 3D printer with a finer layer resolution of 20 µm as shown in Fig. 4(a, b). The 3D-printed bowtie antenna was transferred into an isopropanol (IPA) bath for cleaning for 5 min, then dried with compressed air. A sacrificial photoresist layer of S1805 (Micro posit) was carefully coated to the gap between the ground plane and the CPW line, as shown in Fig. 4(c), then dried in a 50 °C convection oven for 2 min. A lower baking temperature was utilized to prevent unwanted warping or potential deformation of the substrate during the baking process. 100 nm of titanium (Ti) and 300 nm of copper (Cu) seed layers were deposited on both the top and bottom sides of the bowtie antenna and substrate using a DC sputter, as illustrated in Fig. 4(d, e). The seed layers that were deposited at the edge of the substrate were removed using 3000-grit sandpaper. A conventional metal lift-off technique was performed to remove the seed layers deposited inside the gap, allowing the CPW line to be disconnected from the ground plane, as shown in Fig. 4(f). The copper seed layer thickness was increased to 30 µm via copper electroplating with a current density of 10 mA/cm$^2$ to achieve a smooth surface with a slower electroplating rate, as shown in Fig. 4(g, h). After the electroplating process, the sample underwent thorough rinsing in deionized (DI) water and dried with compressed nitrogen gas to prevent oxidation, and the bowtie antenna was on the substrate on the opposite side of the CPW plane as shown in Fig. 4(i). Also, the monopole antenna was manufactured using the same process as outlined for the fabrication of the bowtie antenna.

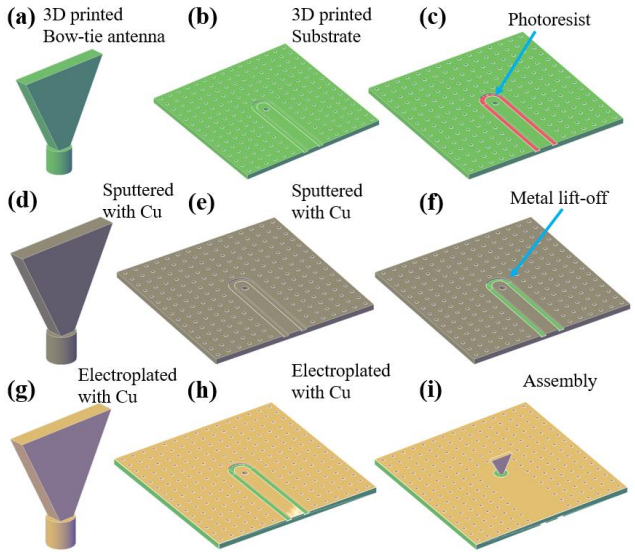


Fig. 4. Fabrication process of 3D air-lifted bowtie antenna (a) 3D-printed bowtie antenna (b) 3D-printed substrate, (c) Photoresist coating on trench, (d) DC sputtering on bowtie antenna, (e) DC sputtering on substrate, (f) Lift-off process on substrate, (g) Electroplating on bowtie antenna, (h) Electroplating on substrate, and (i) Bowtie antenna assemble with substrate.

## IV. Results

Fig. 5 shows the fabrication results of the substrate, the air-lifted bowtie, and the monopole antenna. The height and width of the fabricated bowtie antenna were measured to be 1.667 mm and 1.997 mm, respectively, highlighting the accuracy achieved in the manufacturing process, shown in Fig. 5(b). Similarly, the height and diameter of the fabricated monopole antenna were measured to be 3.090 mm and 492 µm, respectively presented in Fig. 5(c). Noteworthy is the inclusion of a 400 µm insert on the substrate, facilitating connectivity to the coplanar waveguide (CPW) line. Furthermore, antennas are strategically disconnected from the ground by a 100 µm depth island, serving to prevent signal interference and maintain signal integrity, as shown in Fig. 5(a). SMA connectors were soldered to the CPW line and ground plane for both antennas using silver epoxy. The fabricated air-lifted bowtie and monopole antennas were tested for their $|S_{11}|$ values using a vector network analyzer (Anritsu 37269D, operational range: 40 MHz to 40 GHz). A two-port standard short-open-load-thru (SOLT) calibration process was

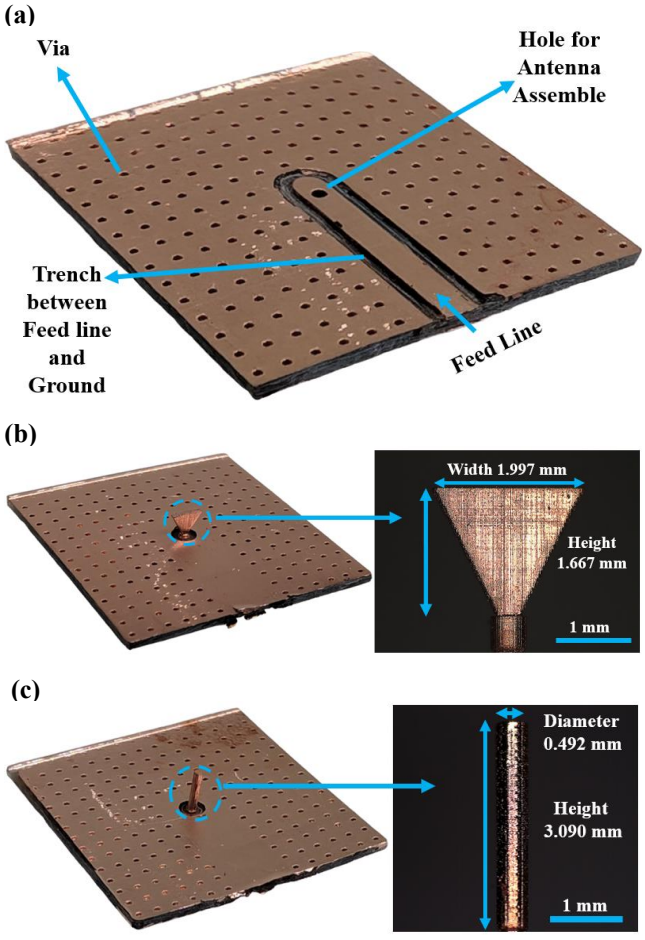


Fig. 5. Fabricated (a) Substrate (b) Bowtie antenna, and (c) Monopole antenna.

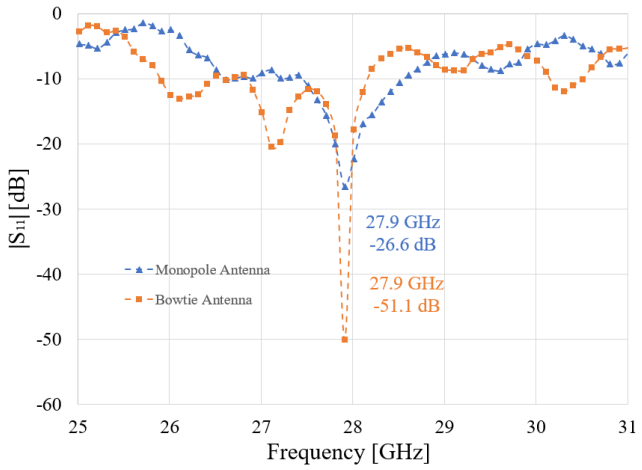


Fig. 6. Measured input reflection coefficients, $|S_{11}|$ [dB], of the fabricated bowtie and monopole antenna.

carried out between 20 GHz and 40 GHz prior to testing to ensure precise readings. The measurement results show that the bowtie and monopole antennas have similar resonant frequencies of 27.9 GHz with measured $|S_{11}|$ values of -51.1 dB and -26.6 dB, respectively, as shown in Fig. 6. While the bowtie antenna showed the same resonance frequency of about 27.9 GHz in both simulation and measurement, the monopole antenna exhibited a slight frequency shift from the simulated value of 28.2 GHz to the measured value of 27.9 GHz. Nonetheless, there was a discrepancy in the simulated and measured bandwidths for both antennas. For the bowtie antenna, the measured bandwidth is around 1.3 GHz, but the simulation indicated a wider bandwidth. The monopole antenna also showed a smaller bandwidth of 1.9 GHz compared to the simulated bandwidth of about 9 GHz.

Fig. 7 shows the measurement data illustrating the achieved enhancement in E-planes and H-planes for both 3D bowtie and monopole antennas. A near-field measurement system placed inside an anechoic chamber was used to precisely measure the radiation patterns of the antennas. At first, the radiation patterns of the antennas were assessed using a Cu layer that was 5 µm thick. Although the ideal copper thickness for the 28 GHz frequency is around 400 nm, we intentionally selected a larger layer of 5 µm to guarantee excellent conductivity. Nevertheless, it was noted that the radiation patterns were inadequate for efficient signal transmission. As a result, it was decided to enhance the thickness of the Cu, resulting in notable enhancements in the antenna gains. The measurement results demonstrated that the bowtie antenna achieved a maximum realized gain of 5.48 dBi. It also exhibited uniform propagation in the H-plane and enhanced performance in the E-plane, as shown in Fig. 7 (a, b) for a bowtie antenna with 30 µm Cu thickness compared to 5 µm thickness Cu. Similarly, significant improvements were found for the monopole antenna, with a maximum realized gain of 6.19 dBi reached when using a copper thickness of 30 µm as shown in Fig. 7 (c, d). These findings emphasize the significance of adjusting the thickness of copper to improve the radiation patterns and overall performance of 3D antennas in wireless communication systems.

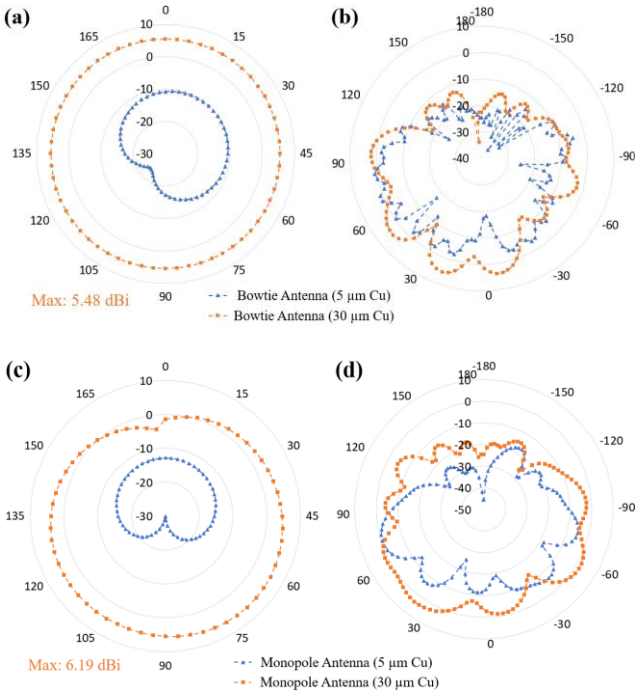


Fig. 7. Measured radiation pattern for the fabricated antennas with thinner and thicker layers of Cu (a) H-plane and (b) E-plane realized gain of the bowtie antenna. (c) H-plane and (d) E-plane realized gain of the monopole antenna.

The minor shift of 0.3 GHz in the resonant frequency of the fabricated monopole antenna prototypes can be attributed to the reduced size of the 3D-printed parts. These results highlight how crucial it is to take the manufacturing process's inherent variability and fabrication tolerances into account when interpreting simulation results and constructing high-frequency antennas.

## V. Conclusion

This study has successfully demonstrated the integration of digital light processing (DLP)-based 3D printing with traditional micromachining techniques for the fabrication of air-lifted bowtie and monopole antennas tailored for the Ka-band, which is vital for next-generation 5G networks. Our research highlights the advantages of using unconventional dielectric materials and advanced fabrication methods to meet the demands of modern wireless communication systems.

The fabricated antennas showcased exemplary performance attributes ideal for high-frequency applications. The air-lifted bowtie antenna, with dimensions of 1.667 mm in height and 1.997 mm in top width, achieved a resonance frequency of 27.9 GHz, $|S_{11}|$ of -51.1 dB, and a maximum realized gain of 5.48 dBi with a 30 µm copper thickness. Similarly, the monopole antenna, measuring 3.09 mm in height and 492 µm in diameter, resonated at the same frequency with $|S_{11}|$ of -26.6 dB and a maximum realized gain of 6.19 dBi. The increase in copper thickness notably enhanced the structural integrity of the antenna components, reducing losses and boosting conductivity—crucial factors for optimizing antenna performance.

These findings underscore the significant advancements that DLP 3D printing technology offers in the fabrication of complex antenna structures, which are both highly efficient and scalable. Future research should explore the application of these innovative design and fabrication techniques across other frequency ranges and in different domains such as radar systems, satellite communications, and the Internet of Things (IoT). By continuing to refine these methods, we can expand the limits of what is possible in antenna technology and wireless communications, paving the way for more sophisticated and robust communication networks.

## ACKNOWLEDGMENT

The research was supported by the National Science Foundation (NSF) CNS 2039014, ECCS 2326938, ECCS 2325032, Korea Evaluation Institute of Industrial Technology (KEIT) 20018023, and Korea Institute for Advancement of Technology (KIAT) P163800009.

## REFERENCES

[1] M. Pons, E. Valenzuela, B. Rodríguez, J. A. Nolazco-Flores, and C. Del-Valle-Soto, "Utilization of 5G Technologies in IoT Applications: Current Limitations by Interference and Network Optimization Difficulties—A Review," *Sensors*, vol. 23, no. 8, p. 3876, Apr. 2023, doi: 10.3390/s23083876.

[2] Y. O. Imam-Fulani *et al.*, "5G Frequency Standardization, Technologies, Channel Models, and Network Deployment: Advances, Challenges, and Future Directions," *Sustainability*, vol. 15, no. 6, Art. no. 6, Jan. 2023, doi: 10.3390/su15065173.

[3] H. El-Hakim and H. Mohamed, "Synthesis of a Multiband Microstrip Patch Antenna for 5G Wireless Communications," *J. Infrared Millim. Terahertz Waves*, vol. 44, pp. 1–17, Aug. 2023, doi: 10.1007/s10762-023-00937-y.

[4] M. Pant and L. Malviya, "Design, developments, and applications of 5G antennas: A review," pp. 156–182, Feb. 2022, doi: 10.1017/S1759078722000095.

[5] Y. Li, Q. Feng, and L. Zhou, "DIPOLE ANTENNA DESIGN FOR PORTABLE DEVICES OPERATING IN THE 5G NR FREQUENCY BANDS," *Prog. Electromagn. Res. Lett.*, vol. 101, pp. 43–48, Jan. 2021, doi: 10.2528/PIERL21090401.

[6] B. Ghassemiparvin and N. Ghalichechian, "Design, fabrication, and testing of a helical antenna using 3D printing technology," *Microw. Opt. Technol. Lett.*, vol. 62, no. 4, pp. 1577–1580, 2020, doi: 10.1002/mop.32184.

[7] S. Y. Jun, B. Sanz-Izquierdo, E. A. Parker, D. Bird, and A. McClelland, "Manufacturing Considerations in the 3-D Printing of Fractal Antennas," *IEEE Trans. Compon. Packag. Manuf. Technol.*, vol. 7, no. 11, pp. 1891–1898, Nov. 2017, doi: 10.1109/TCPMT.2017.2730366.

[8] Y. Wang *et al.*, "3D Printed Antennas for 5G Communication: Current Progress and Future Challenges," *Chin. J. Mech. Eng. Addit. Manuf. Front.*, vol. 2, no. 1, p. 100065, Mar. 2023, doi: 10.1016/j.cjmeam.2023.100065.

[9] Y. Zhang, S. Ogurtsov, V. Vasilev, A. A. Kishk, and D. Caratelli, "Advanced Dielectric Resonator Antenna Technology for 5G and 6G Applications," *Sensors*, vol. 24, no. 5, Art. no. 5, Jan. 2024, doi: 10.3390/s24051413.

[10] J. Kim, X. Cheng, H. Ahn, D. S. Elles, and Y.-K. Yoon, "Lithographically defined integrable air-lifted bow-tie antennas," in *2010 IEEE 23rd International Conference on Micro Electro Mechanical Systems (MEMS)*, Jan. 2010, pp. 791–794. doi: 10.1109/MEMSYS.2010.5442287.

[11] J. Y. Tan, T. Yun, M. Almuslem, and J. J. K. Kim, "3-D Printing Assisted Micromachined RF Patch Antenna," in *2020 IEEE 15th International Conference on Nano/Micro Engineered and Molecular System (NEMS)*, Sep. 2020, pp. 234–237. doi: 10.1109/NEMS50311.2020.9265553.

[12] J. Kim and Y.-K. Yoon, "Fabrication of three-dimensional millimeter-height structures using direct ultraviolet lithography on liquid-state photoresist for simple and fast manufacturing," *J. MicroNanolithography MEMS MOEMS*, vol. 14, no. 3, p. 033504, Jul. 2015, doi: 10.1117/1.JMM.14.3.033504.

[13] A. Pandey, *Practical Microstrip and Printed Antenna Design*. Artech House, 2019.

[14] A. Malas, D. Isakov, K. Couling, and G. J. Gibbons, "Fabrication of High Permittivity Resin Composite for Vat Photopolymerization 3D Printing: Morphology, Thermal, Dynamic Mechanical and Dielectric Properties," *Materials*, vol. 12, no. 23, Art. no. 23, Jan. 2019, doi: 10.3390/ma12233818.